J|A|C|S
ARTICLES
Published on Web 07/12/2006

X-ray Absorption Spectroscopy and Density Functional Theory Studies of $[(H_3buea)Fe^{III}{-}X]^{n-}$ ($X = S^{2-}$, O^{2-}, OH^-): Comparison of Bonding and Hydrogen Bonding in Oxo and Sulfido Complexes

Abhishek Dey,[†] Rosalie K. Hocking,[†] Peter Larsen,[§] Andrew S. Borovik,*[,§] Keith O. Hodgson,*[,†,‡] Britt Hedman,*[,‡] and Edward I. Solomon*[,†]

Contribution from the Department of Chemistry, Stanford University, Stanford, California 94305, Department of Chemistry, Kansas University, Lawrence, Kansas 66045, and Stanford Synchrotron Radiation Laboratory, SLAC, Stanford University, Menlo Park, California 94025

Received March 8, 2006; E-mail: aborovik@ku.edu; hogdson@slac.stanford.edu; hedman@slac.stanford.edu; edward.solomon@stanford.edu

Abstract: Iron L-edge, iron K-edge, and sulfur K-edge X-ray absorption spectroscopy was performed on a series of compounds $[Fe^{III}H_3buea(X)]^{n-}$ ($X = S^{2-}$, O^{2-}, OH^-). The experimentally determined electronic structures were used to correlate to density functional theory calculations. Calculations supported by the data were then used to compare the metal−ligand bonding and to evaluate the effects of H-bonding in $Fe^{III}{-}O$ vs $Fe^{III}{-}S$ complexes. It was found that the $Fe^{III}{-}O$ bond, while less covalent, is stronger than the $Fe^{III}{-}S$ bond. This dominantly reflects the larger ionic contribution to the $Fe^{III}{-}O$ bond. The H-bonding energy (for three H-bonds) was estimated to be −25 kcal/mol for the oxo as compared to −12 kcal/mol for the sulfide ligand. This difference is attributed to the larger charge density on the oxo ligand resulting from the lower covalency of the Fe−O bond. These results were extended to consider an $Fe^{IV}{-}O$ complex with the same ligand environment. It was found that hydrogen bonding to $Fe^{IV}{-}O$ is less energetically favorable than that to $Fe^{III}{-}O$, which reflects the highly covalent nature of the $Fe^{IV}{-}O$ bond.

Introduction

Hydrogen bonding is thought to play an important role in modulating the reactivity of many chemical and biological systems by tuning substrate binding and active site geometric and electronic structure.[1,2] Many active sites have highly conserved H-bonds which appear to be key to function as their mutation greatly reduces reactivity.[3] The functional role of these H-bonds has been extensively investigated using different experimental and computational techniques.[4] There are few studies addressing the effects of H-bonding on the electronic structure of inorganic complexes and, in particular, active sites having sulfur ligands.[5−9]

Fe−O and Fe−S bonds are present or thought to be present at the active sites in a large variety of proteins having a wide range of activities. While active sites using Fe−O bonds are mainly involved in O_2 activation (e.g. oxygenases), Fe−S sites are mainly involved in electron transfer (rubredoxins, feredoxins, etc.). There are also a number of catalytic Fe−S active sites (P450, superoxide reductase, nitrile hydratase, etc.) that are important in nature.[10−12] All of these sites show multiple H-bonding interactions from the protein backbone to the O or S ligand that are thought to play vital roles in tuning the active site reactivity. The importance of H-bonds in biomolecules has inspired the design of synthetic ligands that satisfy the valence requirements of a transition metal ion and also provide specific H-bonding environments. For example, numerous porphyrin complexes have been reported that place H-bond donors proximal to an iron center in order to mimic the active sites of hemoglobin, myobglobin, and cytochrome C oxidase.[13,14] More

[†] Department of Chemistry, Stanford University.
[§] Kansas University.
[‡] Stanford Synchrotron Radiation Laboratory, Stanford University.

(1) Steiner, T. *Angew. Chem., Int. Ed.* **2002**, *41*, 48−76.
(2) Hobza, P.; Havlas, Z. *Chem. Rev.* **2000**, *100*, 4253−4264.
(3) (a) Lipscomb, W. N.; Strater, N. *Chem. Rev.* **1996**, *96*, 2375−2433. (b) Bhaumik, D.; Medin, J.; Gathy, K.; Coleman, M. S. *J. Biol. Chem.***1993**, *268*, 5464−5470. (c) Sideraki, V.; Mohamedali, K. A.; Wilson, D. K.; Chang, Z.; Kellems, R. E.; Quiocho, F. A.; Rudolph, F. B. *Biochemistry* **1996**, *35*, 7862−7872.
(4) (a) Kumar, G. A.; Pan, Y. P.; Smallwood, C. J.; McAllister, M. A. *J. Comput. Chem.* **1998**, *19*, 1345−1352. (b) Francois, S.; Rohmer, M. M.; Benard, M.; Moreland, A. C.; Rauchfuss, T. B. *J. Am. Chem. Soc.* **2000**, *122*, 12743−12750.
(5) Yang, X.; Niu, S. Q.; Ichiye, T.; Wang, L. S. *J. Am. Chem. Soc.* **2004**, *126*, 15790−15794.
(6) Torres, R. A.; Lovell, T.; Noodleman, L.; Case, D. A. *J. Am. Chem. Soc.* **2003**, *125*, 1923−1936.
(7) (a) Ueno, T.; Ueyama, N.; Nakamura, A. *J. Chem. Soc., Dalton Trans.* **1996**, *19*, 3859−3863. (b) Ueyama, N.; Yamada, Y.; Okamura, T.; Kimura, S.; Nakamura, A. *Inorg. Chem.* **1996**, *35*, 6473−6484.
(8) Hung, W. P.; Dewan, J. C.; Tuckerman, M.; Walters, M. A. *Inorg. Chim. Acta* **1999**, *291*, 388−394.
(9) Huang, J.; Dewan, J. C.; Walters, M. A. *Inorg. Chim. Acta* **1995**, *228*, 199−206.
(10) Meunier, B.; de Visser, S. P.; Shaik, S. *Chem. Rev.* **2004**, *104*, 3947−3980.
(11) (a) Lee, S. C.; Holm, R. H. *Chem. Rev.* **2004**, *104*, 1135−1157. (b) Rao, P. V.; Holm, R. H. *Chem. Rev.* **2004**, *104*, 527−559.
(12) Endo, I.; Nojiri, M.; Tsujimura, M.; Nakasako, M.; Nagashima, S.; Yohda, M.; Odaka, M. *J. Inorg. Biochem.* **2001**, *83*, 247−253.
(13) Collman, J. P.; Gagne, R. R.; Gray, H. B.; Hare, J. W. *J. Am. Chem. Soc.* **1974**, *96*, 6522−6524.
(14) Kim, E.; Chufan, E. E.; Kamaraj, K.; Karlin, K. D. *Chem. Rev.* **2004**, *104*, 1077−1134.

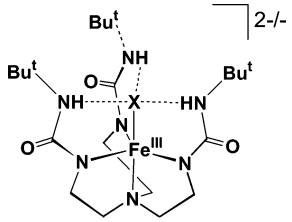

Figure 1. Diagram of the $[Fe^{III}H_3buea(X)]^{n-}$ complexes used for this study.

recently, tripodal ligands have been developed that position H-bond donors near vacant coordination sites of a metal ion.[15] The urea-based tripod ($[H_3buea]^{3-}$) depicted in Figure 1 is one such example and has been used to prepare Fe^{III} complexes with terminal oxo, hydroxo, and sulfido ligands.[16−18] These complexes provide the unique opportunity to compare the electronic structures of monomeric complexes containing Fe^{III}—X (X = O^{2-}, OH^-, S^{2-}) bonds that have the same primary and secondary coordination spheres. Moreover, they allow evaluation of the effects that H-bonds have on the properties of iron complexes with these terminal ligands.

X-ray absorption spectroscopy (XAS) is a powerful physical method that can provide information about the electronic structure of a transition metal site.[19,20] This method is element specific, thereby providing a direct probe of the valence orbitals of the metal center. The ground state of a metal complex is given as a linear combination of metal and ligand valence orbitals. The normalized ground-state wave function is given as

$$\Psi = \alpha|M_{3d}> + \beta|L> + \gamma|M_{4p}> + \delta|M_{4s}> \qquad (1)$$

where α, β, γ, and δ represent the coefficients of the metal 3d, ligand orbital (mainly np), metal 4p, and metal 4s components of the wave function, respectively, and $\beta^2 > 0$ reflects the covalency of the metal−ligand interaction. Metal K-edge XAS provides an estimate of the Z_{eff} (effective nuclear charge) of the metal from the energy position of the "rising-edge" (i.e. $Fe_{1s} \rightarrow Fe_{4p}$) transition. The intensity of the $Fe_{1s} \rightarrow Fe_{3d}$ transition (pre-edge) is a direct measure of the $\%Fe_{4p}$ mixing into the Fe_{3d} orbitals (i.e. γ in eq 1) which, in turn, depends on the geometry of the Fe center. Fe L-edge XAS probes the electric dipole allowed $Fe_{2p} \rightarrow Fe_{3d}$ transitions. The intensity of this feature is directly proportional to, and can be used as a measure of, the $\%Fe_{3d}$ character in the half and unoccupied M_{3d} orbitals (i.e. α^2 in eq 1). S K-edge XAS probes the $S_{1s} \rightarrow S_{4p}$ transition which is indicative of the Z_{eff} on the S atom. Due to covalent mixing of the S_{3p} orbitals into the Fe_{3d} orbitals, a pre-edge feature is also observed in the S K-edge XAS of transition metal complexes whose integrated intensity is directly proportional to, and thus quantifies, the $\%S_{3p}$ character in the half and unoccupied M_{3d} orbitals (i.e. β in eq 1).[21,22] Hence, this combination of XAS techniques can be used to experimentally estimate the ground-state wave function, which can then be used to obtain insight into the electronic structure and its contribution to the reactivity of active sites.

In this study we use Fe K-edge, Fe L-edge, and S K-edge XAS to define the ground-state wave functions of a series of complexes $[(H_3buea)Fe^{III}-X]^{n-}$ (X = S^{2-}, O^{2-}, and OH^-). These experimental descriptions are then used to evaluate the results of density functional theory (DFT) calculations. This combination provides further insight into the nature of Fe−X bonding, where X = O^{2-} and S^{2-} ligands, and the effects of H-bonding on these. This study is further extended to consider the effects H-bonding in a hypothetical Fe^{IV}—oxo system having the same $[H_3buea]^{3-}$ ligand; these results are compared to those for heme−oxo species and used to define the features that may be present in biologically relevant ferryl species.

Experimental Details

Sample Preparation. $[Fe^{III}H_3buea(S)]^{2-}$, $[Fe^{III}H_3buea(O)]^{2-}$, and $[Fe^{III}H_3buea(OH)]^-$ were prepared as described previously.[17,23]

XAS Data Collection. X-ray absorption spectra were recorded at the Stanford Synchrotron Radiation Laboratory (SSRL) on the 31-pole wiggler beam line 10-1 and bending magnet beam line 8-2 (Fe L-edges), bending magnet beam line 2-3 (Fe K-edges), and 54-pole wiggler beam line 6-2 (S K-edge) under ring operating conditions of 70−100 mA and 3 GeV. Details of the beam line optics have been described in previous work.[24−26] For all XAS experiments, samples were prepared in a dry nitrogen-filled glovebox. For Fe L-edge measurements the samples were finely ground and spread across double-sided adhesive conductive graphite tape and attached to a copper paddle, aligned 45° to the incident beam under an inert atmosphere (<0.5 ppm O_2), as described previously.[27] All measurements were made at 20 ± 5 °C. The energy was calibrated from the Fe L-edge spectrum of Fe_2O_3, run at intervals between scans. The second feature in the L_3 and the first feature in the L_2 edges were calibrated to 708.5 and 720.1 eV, respectively. Data were taken over the range 670−830 eV to permit normalization, as described previously.[24] A step size of 0.1 eV was used over the edge region (700−730 eV), and 0.5 eV steps over the remaining regions. Two arc tangents were subtracted from the spectra: absorption = $[\tan^{-1}(k(\text{energy} - I_1) + \pi/2)*2/3*1/\pi] + [\tan^{-1}(k(\text{energy} - I_2) + \pi/2)*1/3*1/\pi]$ where $k = 0.295$ was obtained from the

(15) (a) Harata, M.; Jitsukawa, K.; Masuda, H.; Einaga, H. *J. Am. Chem. Soc.* **1994**, *116*, 10817-10818. (b) Berreau, L. M.; Mahapatra, S.; Halfen, J. A.; Young, V. G., Jr.; Tolman, W. B. *Inorg. Chem.* **1996**, *35*, 6339−6342. (d) Wada, A.; Harata, M.; Hasegawa, K.; Jitsukawa, K.; Masuda, H.; Mukai, M.; Kitagawa, T.; Einaga, H. *Angew. Chem., Int. Ed. Engl.* **1998**, *37*, 798−799. (e) Ogo, S.; Wada, S.; Watanabe, Y.; Iwase, M.; Wada, A.; Harata, M.; Jitsukawa, K.; Masuda, H.; Einage, H. *Angew. Chem., Int. Ed. Engl.* **1998**, *37*, 2102−2104. (f) Garner, D. K.; Allred, R. A.; Tubbs, K. J.; Arif, A. M.; Berreau, L. M. *Inorg. Chem.* **2002**, *41*, 3533−3541. (g) Berreau, L. M.; Makowska-Grzyska, M. M.; Arif, A. M. *Inorg. Chem.* **2000**, *39*, 4390−4391. (h) Garner, D. K.; Fitch, S. B.; McAlexander, L. H.; Bezold, L. M.; Arif, A. M.; Berreau, L. M. *J. Am. Chem. Soc.* **2002**, *124*, 9970−9971. (i) Kitajima, N.; Komatsuzaki, H.; Hikichi, S.; Osawa, M.; Moro-oka, Y. *J. Am. Chem. Soc.* **1994**, *116*, 11596-11597. (j) Hammes, B. S.; Luo, X.; Carrano, M. W.; Carrano, C. J. *Angew. Chem., Int. Ed. Eng.* **2002**, *41*, 3259. (k) Cheruzel, L. E.; Wang, J.; Mashuta, M. S.; Buchanan, R. M. *Chem. Commun.* **2002**, 2166−2167.
(16) McBeth, C. E.; Golombek, A. P.; Young, V. G.; Cheng, Y.; Kuczera, K.; Henderich, M. P.; Borovik, A. S. *Science* **2000**, *289*, 938−941.
(17) Larsen, P. L.; Gupta, R.; Powell, D. R.; Borovik, A. S. *J. Am. Chem. Soc.* **2004**, *126*, 6522−6523.
(18) Borovik, A. S. *Acc. Chem. Res.* **2005**, *38*, 54−61.
(19) *X-ray Absorption: Principles, Applications, Techniques of EXAFS, SEXAFS and XANES*; Koningsberger, D. C., Prins, R., Eds.; John Wiley & Sons: New York, 1988; Vol. 92.
(20) Zhang, H. H.; Hedman, B.; Hodgson, K. O. In *Inorganic Electronic Structure and Spectroscopy*; Solomon, E. I., Lever, A. B. P., Eds.; John Wiley & Sons: New York 1988; Vol. 92.
(21) Glaser, T.; Hedman, B.; Hodgson, K. O.; Solomon, E. I. *Acc. Chem. Res.* **2000**, *33*, 859−869.
(22) Solomon, E. I.; Hedman, B.; Hodgson, K. O.; Dey, A.; Szilagyi, R. K. *Coord. Chem. Rev.* **2005**, *249*, 97−129.
(23) MacBeth, C. E.; Gupta, R.; Mitchell-Koch, K. R.; Young, V. G., Jr.; Lushington, G. H.; Thompson, W. H.; Hendrich, M. P.; Borovik, A. S. *J. Am. Chem. Soc.* **2004**, *126*, 2556−2567.
(24) Wasinger, E. C.; de Groot, F. M. F.; Hedman, B.; Hodgson, K. O.; Solomon, E. I. *J. Am. Chem. Soc.* **2003**, *125*, 12894−12906.
(25) Westre, T. E.; Kennepohl, P.; DeWitt, J. G.; Hedman, B.; Hodgson, K. O.; Solomon, E. I. *J. Am. Chem. Soc.* **1997**, *119*, 6297−6314.
(26) Hedman, B.; Frank, P.; Gheller, S. F.; Roe, A. L.; Newton, W. E.; Hodgson, K. O. *J. Am. Chem. Soc.* **1988**, *110*, 3798−3805.
(27) DeBeer George, S.; Metz, M.; Szilagyi, R. K.; Wang, H.; Cramer, S. P.; Lu, Y.; Tolman, W. B.; Hedman, B.; Hodgson, K. O.; Solomon, E. I. *J. Am. Chem. Soc.* **2001**, *123*, 5757−5767.

experimental fit[5,6] and $I_2 = I_1 + 12.3$ eV (where I_2 is the energy of the L_2 feature relative to that of I_1 of L_3, split by spin−orbit coupling) was used to model the L_3 and L_2 edge jumps, as described previously.[5] The error reported represents the range of integrated intensity, calculated as above, based on at least three repeat measurements of the same spectra on different dates.

For Fe K-edges the samples of each of the compounds were mixed with boron nitride and ground into a fine powder. The powder was loaded into a 1 mm thick Al spacer and sealed with 63.5 μm Mylar tape windows. Fe K-edges were measured in transition mode with N_2-filled ionization chambers to $k = 9.5$ Å^{-1}. A total of 2−3 scans were measured per sample to ensure reproducibility. Energies were calibrated against the first inflection point at 7111.2 eV of an internal foil standard.[28] A second order polynomial was fit to the pre-edge and subtracted from the data. A two-segment spline of order two was fit to the EXAFS region, and all data were normalized to the edge jump at 7130 eV.

For S K-edge XAS experiments the samples were ground into a fine powder and dispersed as thinly as possible on sulfur-free Mylar tape. This procedure has been verified to minimize self-absorption effects. The sample was then mounted across the window of an aluminum plate. A 6.35 μm polypropylene film window protected the solid samples from exposure to air during transfer from the glovebox to the experimental sample chamber.

Fitting Procedure. Fits to the Fe and S K-edges were performed using the program EDG_FIT.[29] Second derivative spectra were used as guidance to determine the number and position of peaks. Pre-edge features were fit using pseudo-Voigt line shapes (sums of Lorentzian and Gaussian functions). This line shape is appropriate as the experimental features are a convolution of a Lorentzian transition envelope and a Gaussian line shape imposed by the beam-line optics.[30,31] A fixed 1:1 ratio of Lorentzian to Gaussian contribution successfully reproduced the pre-edge features. The rising edge functions were also fit with pseudo-Voigt line shapes. Good fits reproduce the data using a minimum number of peaks. Fe K-edge fits were performed over several energy ranges as described in reference 27. The reported intensity values and standard deviations are based on the average of all good fits. Normalization procedures can introduce a ∼3% error in pre-edge peak intensities in addition to the error resulting from the fitting procedure.[32]

DFT Computational Details. All calculations were performed on dual-CPU Pentium Xeon 2.8 GHz work stations and a SGI Origin 2000 computer using the Amsterdam Density Functional (ADF) program, versions 2004.01 and developed by Baerends et al.[33,34] For optimizations, a triple-ζ Slater-type orbital basis set (ADF basis set TZP) with a single polarization function at the local density approximation of Vosko, Wilk, and Nusair[35] with nonlocal gradient corrections of Becke[36] and Perdew[37] were employed. The molecular orbitals were plotted using Gopenmol ver.2.2, and the Mulliken[38] population analyses reported were obtained from the output of the ADF program. For the energy level diagrams the energies of the d orbitals in different complexes (which have different charges) are referenced to the terminal C−H bonding orbitals of the ligand. Energies were estimated by performing single-point calculations on the optimized geometries using the 6-311+G* basis set with the Gaussian 03 package.[39] The solvation calculations were performed using the PCM[40] model with CH_2Cl_2 as solvent. These numbers were also estimated using the COSMO[41] solvation model in the ADF package using an ϵ of 8.9 for CH_2Cl_2, which gave very similar results.

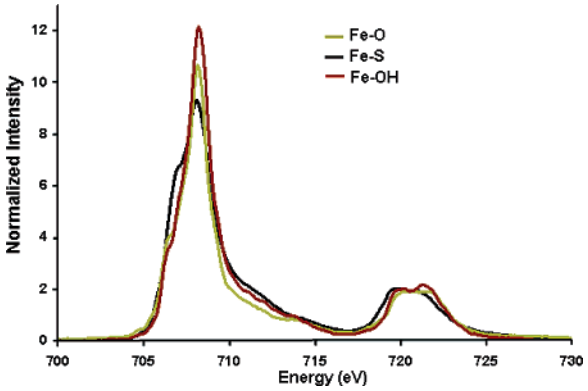

Figure 2. Fe L-edge data of the three compounds $[Fe^{III}H_3buea(S)]^{2-}$ (black, Fe−S), $[Fe^{III}H_3buea(O)]^{2-}$ (green, Fe−O), and $[Fe^{III}H_3buea(OH)]^{-}$ (brown, Fe−OH).

Results

A. XAS. Metal L-Edge XAS. The Fe L-edge spectra of $[Fe^{III}H_3buea(S)]^{2-}$ (black), $[Fe^{III}H_3buea(O)]^{2-}$ (green), and $[Fe^{III}H_3buea(OH)]^{-}$ (brown) are shown in Figure 2. All three compounds have 42 ± 5 units of intensity (Table 1) corresponding to ∼68(9)% Fe_{3d} character per orbital implying that, within error, the unoccupied d character on the metal is very similar for all three compounds.[42] The Fe L-edge intensity-weighed energy positions and branching ratios (Table 1) are typical of those determined for other high-spin Fe^{III} compounds.[25]

Fe K-Edge. The Fe K-edges of $[Fe^{III}H_3buea(S)]^{2-}$, $[Fe^{III}H_3buea(O)]^{2-}$, and $[Fe^{III}H_3buea(OH)]^{-}$ exhibit pre-edge transitions[25] at ∼7113 eV (Figure 3, expanded scale inset). The intensity of this transition is mostly derived from and reflects the mixing of Fe_{4p} character into the unoccupied Fe_{3d} manifold. Weaker quadrupole allowed $Fe_{1s} \rightarrow Fe_{3d}$ transitions also contribute to this intensity. Their relative contributions can be quantified by fits to the data and background (Table 2, Figure S1, Supporting Information). The total intensities of $[Fe^{III}H_3buea(S)]^{2-}$, $[Fe^{III}H_3buea(O)]^{2-}$, and $[Fe^{III}H_3buea(OH)]^{-}$ are 21.6, 27.7, and 25.2, respectively (Table 2), which are relatively high compared to those of other high-spin Fe^{III} complexes. For example, Fe(salen)Cl, which is also five coordinate, has 14 units of pre-edge intensity.[43]

$[Fe^{III}H_3buea(O)]^{2-}$ has less Fe−K pre-edge intensity, and the intensity distribution is broader relative to the pre-edges of $[Fe^{III}H_3buea(S)]^{2-}$ and $[Fe^{III}H_3buea(OH)]^{-}$. The Fe−K pre-edge spectrum of $[Fe^{III}H_3buea(O)]^{2-}$ was fit (Figure S1, Supporting

(28) Scott, R. A.; Hahn, J. E.; Doniach, S.; Freeman, H. C.; Hodgson, K. O. *J. Am. Chem. Soc.* **1982**, *104*, 5364−5369.
(29) EDG_FIT: G. N. George, Stanford Synchrotron Radiation Laboratory, Stanford Linear Accelerator Center, Stanford University, Stanford, CA., 2001.
(30) Agarwal, B. K. In *X-ray Spectroscopy*; Springer-Verlag: Berlin, 1979.
(31) Tyson, T. A.; Roe, A. L.; Frank, P.; Hodgson, K. O.; Hedman, B. *Phys. Rev. B* **1989**, *39A*, 6305−6315.
(32) Thole, B. T.; van der Laan, G. *Phys. Rev.* **1988**, *38B*, 3158−3170.
(33) Baerends, E. J.; Ellis, D. E.; Ros, P. *Chem. Phys.* **1973**, *2*, 41−51.
(34) te Velde, G.; Baerends, E. J. *Int. J. Comput. Phys.* **1992**, *99*, 84−98.
(35) Vosko, S. H.; Wilk, L.; Nusair, M. *Can. J. Phys.* **1980**, *58*, 1200−1211.
(36) Becke, A. D. *Phys. Rev. A: Gen. Phys.* **1988**, *38*, 3098−3100.
(37) Perdew, J. P. *Phys. Rev. B* **1986**, *33*, 8822−8224.
(38) Mulliken, R. S. *J. Chem. Phys.* **1955**, *23*, 1833−1840.
(39) Pople, J. A. et al. *Gaussian 03*, Revision C.02; Gaussian, Inc.: Wallingford, CT, 2004. (Full reference in Supporting Information.)
(40) Miertus, S.; Scrocco, E.; Tomasi, J. *Chem. Phys.* **1981** *55*, 117−129.
(41) Klamt, A.; Schüürmann, G. *J. Chem. Soc.: Perkin Trans.* **1993**, *2*, 799−805.
(42) From the figure it is clear that while the amplitude of the $[Fe(H_3buea)S]^{2-}$ compound is the smallest of the three, it is also broader.
(43) Note that large pre-edge intensity has been observed in high-valent Fe species, e.g. a high-valent $Fe^{V}N$ species has been reported with a pre-edge intensity of 27 units of intensity (Aliaga-Alcalde et al. *Angew. Chem., Int. Ed.* **2005**, *44*, 2908−2912) and $Fe^{IV}O$ species typically have intensities of around 25 units (Rohde et al. *J. Am. Chem. Soc.* **2004**, *126*, 16750−16761). However, these species are Fe(IV) and Fe(V) and thus have more holes in the d manifold.

Table 1. Summary of Results from Fe L-Edge Experimental Data[a]

	total intensity	total orbital covalency (%)	intensity-weighted avg energy and intensity (L_3, L_2) (eV)	branching ratio $L_3/(L_2+L_3)$
$[Fe^{III}H_3buea(O)]^{2-}$	41 (6)	67 (10)	708.48 (31.1), 720.18 (9.54)	0.77 (0.02)
$[Fe^{III}H_3buea(S)]^{2-}$	44 (5)	69 (7)	708.35 (34.4), 720.95 (9.6)	0.78 (0.02)
$[Fe^{III}H_3buea(OH)]^{-}$	43 (5)	67 (8)	708.40 (34.3), 720.96 (8.74)	0.80 (0.02)

[a] Estimated errors are given in parentheses.

Table 2. Summary of Results from Fe K-Edge Experimental Data[a]

	total intensity	intensity-weighted avg energy	peak contributions [area]	%p mixing
$[Fe^{III}H_3buea(O)]^{2-}$	21.6 (0.3)	7113.4 (0.12)	7112.8 [9.56], 7113.9 [11.64]	14.9 (6.6)
$[Fe^{III}H_3buea(S)]^{2-}$	27.7 (0.3)	7113.0 (0.05)	7112.9 [17.74], 7113.8 [3.96]	19.9 (8.5)
$[Fe^{III}H_3buea(OH)]^{-}$	25.2 (0.3)	7113.4 (0.03)	7113.4 [25.2]	17.9 (7.7)

[a] Estimated errors are given in parentheses.

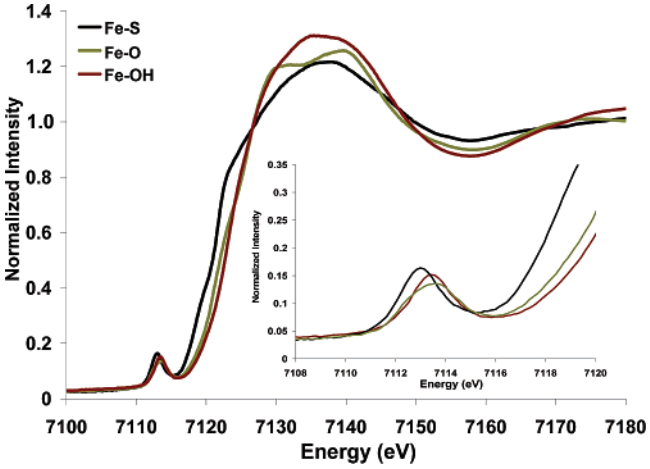

Figure 3. Fe K-edge data of the three compounds $[Fe^{III}H_3buea(S)]^{2-}$ (black, Fe−S), $[Fe^{III}H_3buea(O)]^{2-}$ (green, Fe−O), and $[Fe^{III}H_3buea(OH)]^{-}$ (red, Fe−OH). The inset highlights the pre-edges.

Information) with two peaks of approximately equal intensity (9.6 and 11.6 units) spaced 1.1 eV apart at 7113.8 and 7113.9 eV (Table 2). The $[Fe^{III}H_3buea(S)]^{2-}$ feature was also fit with two peaks, which were 1.0 eV apart, with most of the intensity (17.7 units) concentrated in one peak at 7112.9 eV, and the $[Fe^{III}H_3buea(OH)]^{-}$ pre-edge was fit well with just one peak at 7113.4 eV having 25.2 units of intensity. These differences reflect ligand field effects at the Fe^{III} center (vide infra).

Ligand K-Edge XAS. The S K-edge XAS of the $[Fe^{III}H_3buea(S)]^{2-}$complex shows an intense pre-edge transition at 2469.8 eV (Figure 4). This feature is assigned to an envelope of $S_{1s}\rightarrow Fe_{3d}$ transitions. The intensity is proportional to the $\%S_{3p}$ mixed into the five singly occupied Fe_{3d} orbitals. Fitting the data gives a pre-edge intensity of 2.3 ± 0.05 units which corresponds to 82% S_{3p} orbital character summed over the five half-occupied Fe_{3d} orbitals (calibration is described in reference 44). As a reference, the S K-edge spectrum of two well-studied complexes, $Et_4N[Fe^{III}(SPh)_4]$ and $(Et_4N)_2[Fe^{III}_2S_2Cl_4]$, are included in Figure 3. The higher intensity of $[Fe(H_3buea)S]^{2-}$ relative to these references indicate that the terminal sulfide is more covalent than a bridging sulfide or a terminal thiolate.

B. DFT Calculations. Geometry optimized DFT calculations were performed on the three complexes. While the optimized

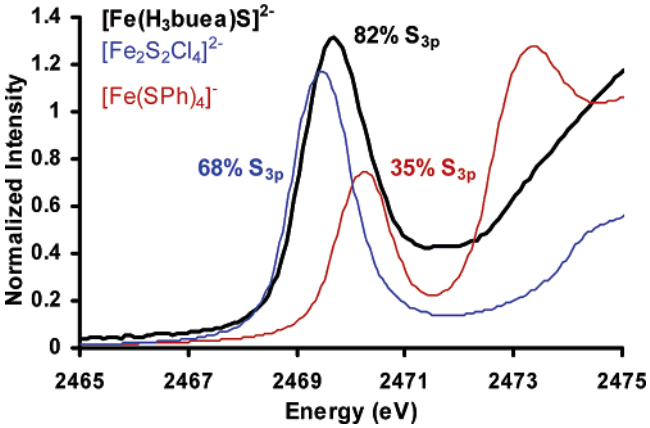

Figure 4. S K-edge XAS of $[Fe^{III}H_3buea(S)]^{2-}$ (black, terminal $S_{sulfide}$), $[Fe^{III}(SPh)_4]^{-}$ (red, terminal $S_{thiolate}$), and $[Fe^{III}_2S_2Cl_4]^{2-}$ (blue, $\mu_2S_{sulfide}$).

Fe−X and the $Fe-N_{equatorial}$ bond lengths and angles are in good agreement with the published crystallographic data (Table 3), the $Fe-N_{axial}$ distances are longer in the optimized structures. The NH···X distances are well reproduced and are about 0.6 Å shorter in the Fe−O and Fe−OH complexes than in the Fe−S complex.

The MO diagrams for the $[Fe^{III}H_3buea(O)]^{n-}$ (X = O, S, and OH) complexes (Figure 5) show a trigonal ligand field splitting of the d orbitals. The d_{z^2} orbital has a σ interaction with the axial ligand X and with the N_{axial} $2p_z$ orbital, the latter being a relatively weak ligand due to its longer $Fe-N_{axial}$ distance. The $d_{yz,xz}$ and the $d_{x^2-y^2,xy}$ orbitals (both sets transform as E in C_3 symmetry) mix with each other, as the Fe is shifted out of the equatorial plane and has π interactions with the $np_{x,y}$ orbitals available on the X ligand (x,y also transform as E in C_3). The sulfido complex is more covalent than the oxo complex based on the sum of the ligand np orbital character in the half-occupied (i.e. β unoccupied in spin unrestricted calculation) Fe_{3d} orbitals (61% S_{3p} vs 49% O_{2p}). Note that the additional π interactions available for terminal oxo and sulfido ligands increases the Fe−X bond covalency and decreases the Fe−X bond length relative to HO^- or RS^- ligands where one of the np orbitals is involved in the O−H/S−C σ bond.

The MO calculations indicate that there is about 6%, 7%, and 8% Fe_{4p} mixing in these Fe_{3d} orbitals in the oxo, sulfido, and hydroxo complexes, respectively. This Fe_{4p} mixing into the Fe_{3d} based orbitals provides a mechanism for introduction of

(44) Rose, K.; Shadle, S. E.; Glaser, T.; de Vries, S.; Cherepanov, A.; Canters, G. W.; Hedman, B.; Hodgson, K. O.; Solomon, E. I. *J. Am. Chem. Soc.* **1999**, *121*, 2353−2363.

Table 3. Optimized Geometric Parameters[a]

	Fe–X (Å)	Fe–N_{ax}[b] (Å)	Fe–N_{eq}[b] (Å)	X–Fe–N_{eq} (deg)	N_{eq}–Fe–N_{eq} (deg)	NHX (Å)
$[Fe^{III}H_3buea(O)]^{2-}$	1.81	2.28	2.10	104	113−112	2.75
$[Fe^{III}H_3buea(O)]^{2-}$	(1.81)	(2.44)	(2.05)	(101)	(119)	(2.70)
$[Fe^{III}H_3buea(S)]^{2-}$	2.23	2.79	2.07	109	108−103	3.34
$[Fe^{III}H_3buea(S)]^{2-}$	(2.20)	(2.65)	(2.03)	(106−109)	(119−106)	(3.35)
$[Fe^{III}H_3buea(OH)]^{-}$	1.96	2.55		104	118−108	2.94−3.12

[a] Crystallographic data in parentheses. [b] N_{eq} and N_{ax} are the equatorial and axial nitrogen ligands, respectively.

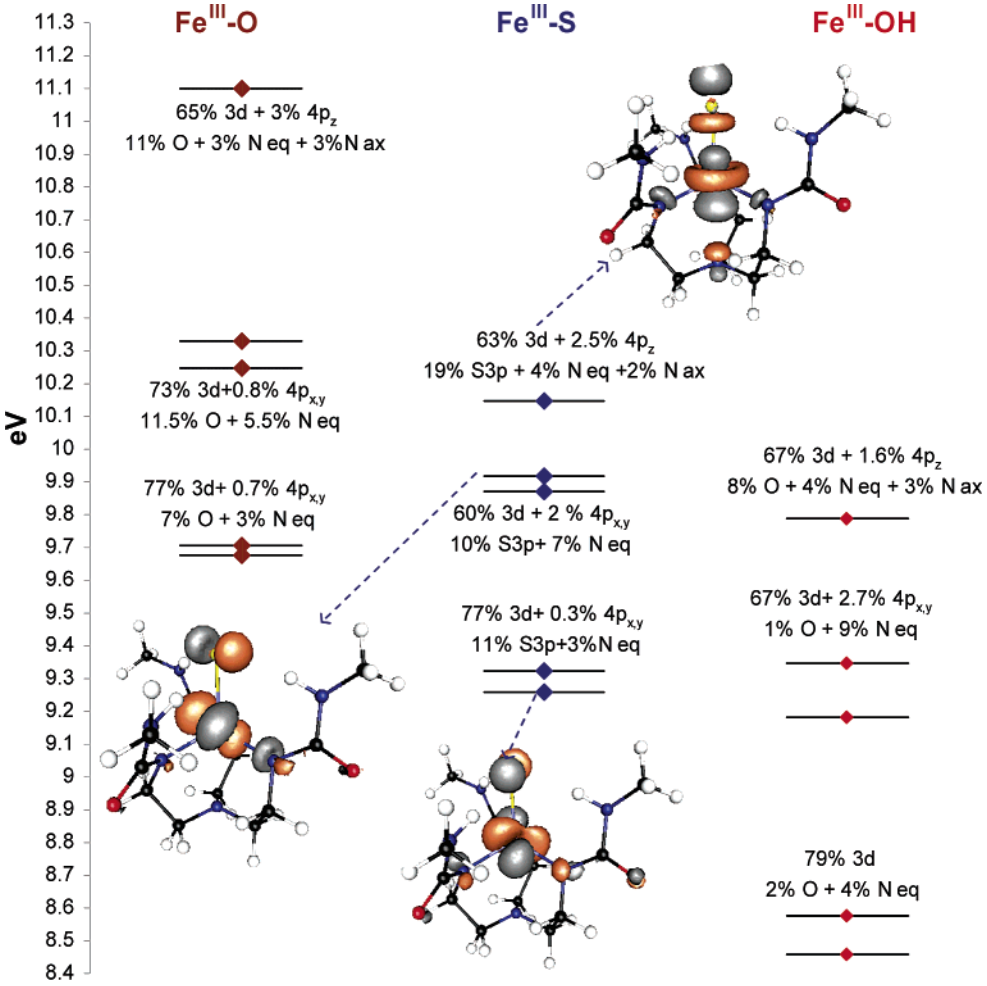

Figure 5. MO diagram of $[Fe^{III}H_3buea(O)]^{2-}$, $[Fe^{III}H_3buea(S)]^{2-}$, and $[Fe^{III}H_3buea(OH)]^{-}$ showing the β-unoccupied orbitals. The coefficients (average values for the E set) of Fe_{3d} (3d), Fe_{4p} (4p), X_{np} (np), $N_{ax\ 2p}$ (N ax), and $N_{eq\ 2p}$ (N eq) and representative contour diagrams for individual sets of d orbitals are given.

intensity into the pre-edge of the Fe K-edge XAS. The orbital splitting pattern and the 4p character distribution in these orbitals and the relative covalencies of the complexes from the Fe K-edge, Fe L-edge, and S K-edge data are used below to experimentally evaluate these DFT calculations. These calculations will then be used to estimate the effects of H-bonding in the $Fe^{III-}O$ and the $Fe^{III-}S$ complexes.

Analysis

A. Evaluation of DFT Calculations Using XAS. Properties of the ground-state wave functions obtained from the geometry optimized DFT calculations at the BP86 level are tabulated in Table 4. The average Fe_{3d} character per hole is calculated to be 67%, 72%, and 72% for $[Fe^{III}H_3buea(S)]^{2-}$, $[Fe^{III}H_3buea(O)]^{2-}$, and $[Fe^{III}H_3buea(OH)]^{-}$, respectively. These values are very similar to each other (within ±3%) and in agreement with experiment (Table 4, column 1 in parentheses). MO calculations show that the OH group is less covalent than the S or O group; however, this is compensated by the increase in covalency from the strong amide donors (increase in $\%N_{2p}$ in the Fe_{3d} manifold) and does not result in a significant change in Fe_{3d} population. The $\%S_{3p}$ character in $Fe^{III-}S$ is calculated to be 12% (Table 4, row 2) and is in reasonable agreement with the experimentally observed value of 16% from S K-edge intensity.

The calculations further show that there is significant Fe_{4p} mixing in the two E sets of the Fe_{3d} orbitals.[45] This large mixing is due to the C_3 symmetry axis associated with these complexes. This is in addition to the Fe $4p_z$ mixed into the d_{z^2} orbital due to the lack of inversion along Z. The additional $4p_{x,y}$ orbital mixing is reflected in the higher pre-edge intensity (21−28%)

(45) Note that even though the calculations underestimate the 4p mixing, they reproduce the intensity distribution of the pre-edge feature (vide infra).

Table 4. Calculated Ground-State Properties[a]

	%Fe_{3d} (avg)[b] (from L-edge)	%X_{np}(avg)	%N_{2p} (avg)[b]	%Fe_{4p} E	%Fe_{4p} A	%Fe_{4p} total (from K-edge)[c]	ν_{Fe-X} (cm^{-1})
$[Fe^{III}H_3buea(O)]^{2-}$	72 (67)	10	4	3	3	6 (14.9)	683 (671)
$[Fe^{III}H_3buea(S)]^{2-}$	67 (69)	12 (16)	5	5	2	7 (19.9)	369
$[Fe^{III}H_3buea(OH)]^{-}$	72 (67)	5	6	6	2	8 (17.9)	

[a] Experimental data in parentheses. [b] Summed over all Fe_{3d} orbitals and divided by the number of Fe_{3d} orbitals. [c] Summed over all Fe_{3d} orbitals.

of the $[Fe^{III}H_3buea(X)]^{2-/-}$ complexes compared to $[Fe^{III}$(salen)-Cl], which is only at 14%. The C_4 symmetry in $[Fe^{III}$(salen Cl] greatly reduces the $4p_{x,y}$ mixing with the 3d orbitals and the dominant contribution to the pre-edge intensity comes only from the mixing of the $4p_z$ into d_{z^2}.

Furthermore, the $4p_{x,y}$ mixing is distributed differently between these complexes. In the $[Fe^{III}H_3buea(OH)]^{-}$ complex, the mixing is primarily in the higher energy E orbitals while in the $[Fe^{III}H_3buea(O)]^{2-}$ and $[Fe^{III}H_3buea(S)]^{2-}$ complexes the two E sets of orbitals are mixed as the Fe atom is more out of the equatorial plane in these complexes (~0.56 Å) relative to the $[Fe^{III}H_3buea(OH)]^{-}$ complex (~0.48 Å) resulting in redistribution of the Fe $4p_{x,y}$ character between them. The ligand field splitting is also larger in the oxo (1.4 eV) than in the sulfido (0.9 eV) complex reflecting the stronger interaction of the axial N_{ax} with the d_{z^2} orbital due to the shorter Fe−N_{ax} bond in $[Fe^{III}H_3buea(O)]^{2-}$ (2.5 Å) relative to that of $[Fe^{III}H_3buea(S)]^{2-}$ (2.7 Å). This is reflected in the trend in the Fe K-edge pre-edge splitting: oxo > sulfide > hydroxo. The pre-edge regions of these complexes were simulated (Figure 6) using the DFT-calculated Fe_{3d} and Fe_{4p} characters (scaled by appropriate transition moment integrals for $Fe_{1s}\rightarrow Fe_{3d}$ and $Fe_{1s}\rightarrow Fe_{4p}$) and the energy splittings of the five Fe_{3d} molecular orbitals. These results correlate with the experimental data, as shown in Figure 6, particularly the broadening of the Fe−O pre-edge. Taken together, these results indicate that the DFT calculations have acceptably reproduced the experimental ground-state properties.

B. Comparison of the Fe^{III}—O and Fe^{III}—S Bonding. The evaluation of the Fe−X bond energy and the H-bonding energy in this ligand system is complicated by the fact that the H_3buea ligand can H-bond to itself. To uncouple this effect, the complete model of the H_3buea ligand system (Figure 7A, H-bonded) was modified by eliminating the H-bond donor amide-arms of the ligand (Figure 7B, no H-bond). The H-bonding was then simulated by introducing three H_2O molecules (Figure 7C, H-bond from H_2O) around X in an approximately C_3 arrangement and the geometry of the system was then fully optimized.

Without H-bonding both the Fe^{III}−O and the Fe^{III}−S bonds are very covalent, as evident from the large ligand *n*p mixing into the antibonding Fe_{3d} manifold (73% O_{2p} and 81% S_{3p}, Table 5). The Fe−S bond is more covalent than the Fe−O bond. However, the calculated Fe^{III}−X bond stretching frequencies (681 cm^{-1} for Fe−O and 369 cm^{-1} for Fe−S) indicate that the Fe−X bond force constant of the Fe^{III}−O bond is higher (3.55 mdynes/Å) than that of the Fe^{III}−S bond (1.87 mdynes/Å).[46] Their relative bond strengths are also reflected in their Fe−X bond energies (calculated from fragment dissociation in CH_2Cl_2 solvent), which show that the Fe^{III}−O bond energy is about −102 kcal/mol, significantly higher than the Fe^{III}−S bonding energy of −62 kcal/ mol.[47] Note that, although the coefficients

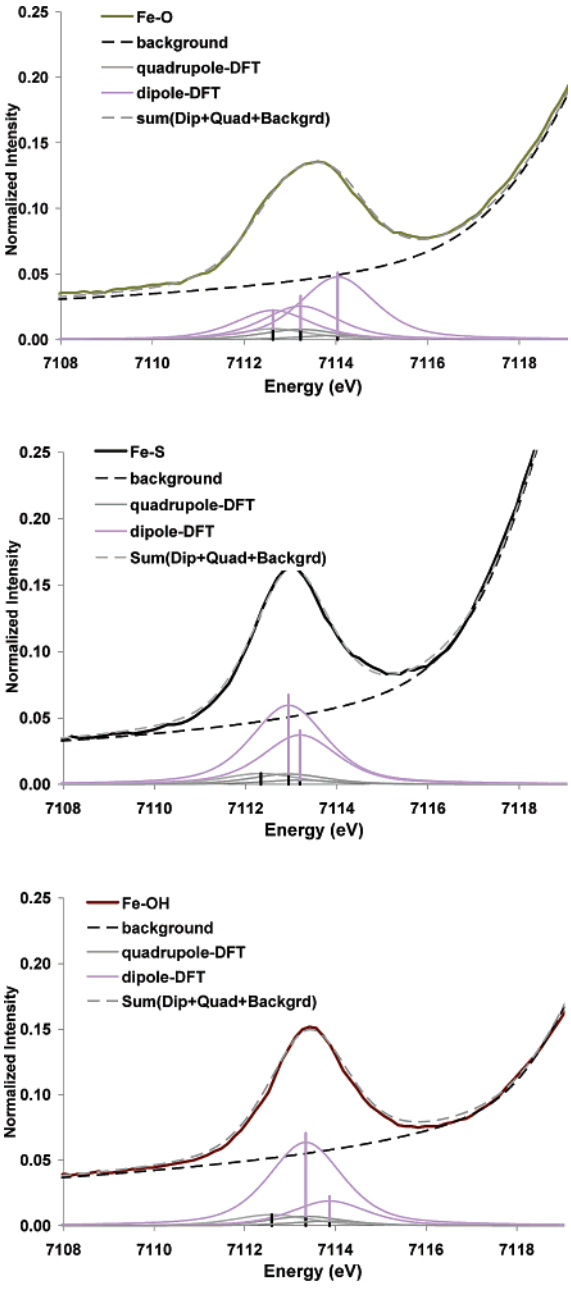

Figure 6. Comparison of the Fe K-edge pre-edge data and Gaussian-broadened DFT-calculated intensities. $[Fe^{III}H_3buea(S)]^{2-}$: Fe−S. $[Fe^{III}H_3buea(O)]^{2-}$: Fe−O. $[Fe^{III}H_3buea(OH)]^{-}$: Fe−OH. Black and purple lines represent the quadrupole and dipole contributions calculated from DFT.

(46) Note that the force constant for Fe−O is expected to be higher than that of Fe−S by a factor of 1.44 due to higher mass of S (32) relative to O (16). However, here the ratio is 1.9 which indicates that the Fe−O bond is stronger than the Fe−S bond.

(47) The bond energies calculated here are ΔE's. To estimate realisitic ΔG's for these reactions one needs to account for the pK_a's of these dianaionic ligands in addition to entropy effects. The ΔE's provide relative binding energy estimates due to differences in bonding.

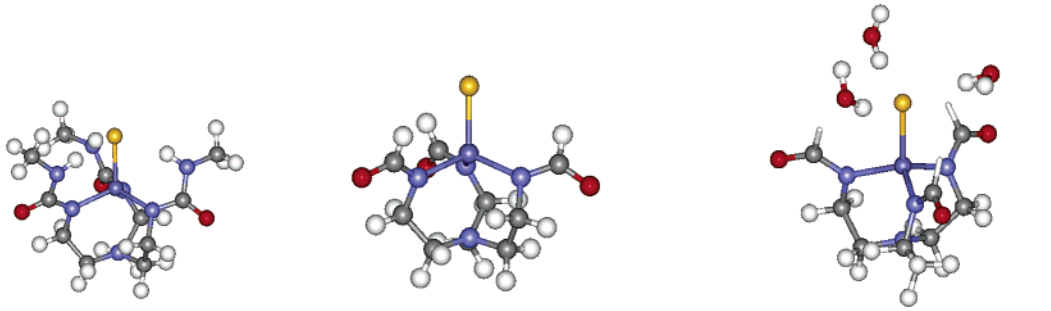

Figure 7. H-bonded and non-H-bonded systems used to evaluate bonding energies.

Table 5. Effect of H-Bonding on O^{2-} vs S^{2-}

		Fe–X (Å)	covalency (%X_{np})	NPA charge Fe	NPA charge X	Fe–X bond energy (kcal/mol)	H-bond energy (kcal/mol)	Fe–X force constant (mdynes/cm^2)
O^{2-}	H-bonded from ligand	1.81	49	2.5	−0.23			2.65
O^{2-}	no H-bond	1.74	73	2.44	−0.01	−102		3.55
O^{2-}	H-bond from H_2O	1.80	46 (57)[a]	2.53	−0.27	−83	−25	
S^{2-}	H-bonded from ligand	2.23	61	2.26	−0.08			1.54
S^{2-}	no H-bond	2.17	81	2.25	0.06	−62		1.87
S^{2-}	H-bond from H_2O	2.21	60 (69)[a]	2.29	−0.12	−55	−12	

[a] Calculations performed using dipoles instead of H_2O molecules.

of mixing indicate that the Fe−S bond is more covalent, the covalent contribution to the bond energy can be approximated by $\alpha^2\Delta$ (where α^2 is the ligand character per orbital and Δ is the energy gap between acceptor Fe^{III} orbitals and the donor X^{2-} orbitals before bonding) and Δ is higher for oxo due to its higher electronegativity. The difference in Δ can be estimated from the O→Fe and S→Fe CT bands of $[Fe^{III}H_3buea(O)]^{2-}$ (at 395 nm) and $[Fe^{III}H_3buea(S)]^{2-}$ (at 575 nm) complexes to be 0.65 eV (higher for oxo, theoretical estimate of 0.8 eV from the DFT calculated ground state). Thus even though α^2 is higher for the Fe^{III}−S complex, the Fe^{III}−O complex has a greater value for Δ, leading to a larger covalent contribution to the bond energy, which is estimated to be 8 kcal/mol more than the Fe−S covalent contribution to the bond energy. The Fe^{III}−O unit also has a larger ionic contribution because of the higher charge density on the iron and oxo centers (which reflects its lower covalency relative to the sulfido), which also contributes to its greater bond energy and force constant. The ionic contribution can be estimated from calculated NPA charges on the ligand atoms coordinated to the Fe^{III} center, which is approximately 25 kcal/mol greater in $[Fe^{III}H_3buea(O)]^{2-}$ than in $[Fe^{III}H_3buea(S)]^{2-}$.[48]

C. Effects of H-Bonding. On going to the H-bonded H_3buea complex (Figure 7B to Figure 6A) the Fe−X bond lengths increase from 1.74 to 1.81 Å for Fe^{III}−O and from 2.17 to 2.23 Å in Fe^{III}−S (Table 5). Associated with these bond length increases, the Fe−X bond covalency is reduced to 49% from 73% in Fe^{III}−O and to 61% from 81% in Fe^{III}−S (Table 5). The same increase in bond length and decrease in covalency on H-bonding is observed in the oxo and sulfido complexes H-bonded to three H_2O molecules (Figure 7B to C and Table 5). The calculated Fe−X force constants for the H-bonded complexes decrease significantly, from 3.55 to 2.65 mdynes/Å for Fe^{III}−O and from 1.87 to 1.54 mdynes/Å for Fe^{III}−S. The increase in the Fe−X distance, decrease of the Fe−X bond covalency, and decrease of the Fe−X bond force constant indicate that the axial H-bonding interaction significantly weakens the Fe−X bond. However, the energy of the H-bonding interaction evaluated from the H_2O H-bonded system (Figure 7C and Table 5) is −25 kcal/mol for the Fe^{III}−O complex and −12 kcal/mol for the Fe^{III}−S complex, indicating that in both cases, despite the weakening of Fe−X bonds, the overall process is energetically favorable.[49,50] Insight into these Fe−X and H-bonding energies can be obtained from the following bond-energy decomposition scheme (Scheme 1).

Scheme 1. Bonding Decomposition Scheme for Fe^{III}−O (top) and Fe^{III}−S (bottom)[a]

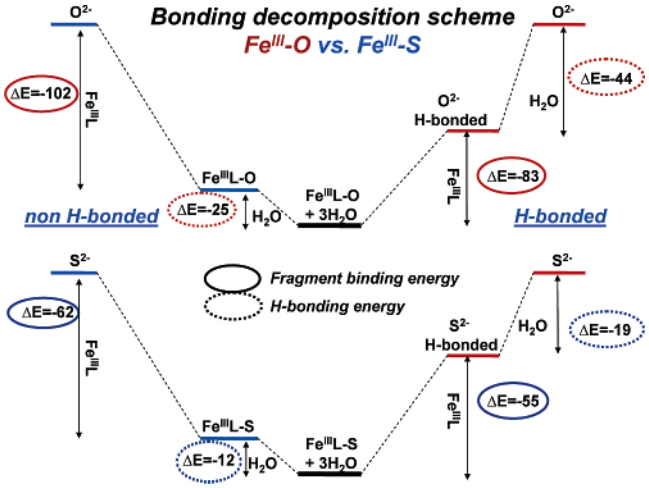

[a] To the left, the non-H-bonded ligand is bound to $Fe^{III}L$ (Fe^{III} bound to the non-H-bonding tetra-dentate ligand L) to form LFe^{III}−X, which is then H-bonded to three H_2O molecules, while to the right the X is first H-bonded to three H_2O molecules and then bound to $Fe^{III}L$. The energies are estimated using a PCM model with CH_2Cl_2 as solvent.

The Fe−X bond energy in absence of the H-bonding (Scheme 1, left) is much higher for Fe^{III}−O (−102 kcal/mol) than for

(48) Note that there will be some contribution to the differences in Fe−O and Fe−S bonding energy from the differences of binding energy of the tridentate ligand between the Fe−O and the Fe−S complexes.

$Fe^{III}-S$ (−62 kcal/mol), and on H-bonding, the systems stabilize by −25 kcal/mol and −12 kcal/mol, respectively. Alternatively, if we first allow for the H-bonding to the O^{2-} and the S^{2-} ions (Scheme 1, right), their bonding energies with the Fe^{III} fragment is significantly reduced to −83 kcal/mol and −55 kcal/mol, respectively. However, the H-bonding energies of the bare O^{2-} and the S^{2-} ions are very high, −44 kcal/mol and −19 kcal/mol, respectively, which compensate for the loss of Fe−X bond energy and result in the overall stabilization of the H-bond (Scheme 1 right, Table 5).[51] The high H-bonding energy of the O^{2-} ion relative to the S^{2-} ion results from the stronger Coulombic interaction of the O^{2-} with the water dipoles as the charge density on the oxo is higher and the H···O distances are about 0.7 Å shorter than the corresponding H···S distances.[52] This dramatic reduction of Fe−X bond energy on H-bonding is reflected in the large increase of Fe−X bond length, reduction of Fe−X bond covalency, and decrease of Fe−X bond force constant. Also the larger reduction of the $Fe^{III}-O$ bond energy as compared to that of the $Fe^{III}-S$ bond contributes to its larger change in these properties.

The reduction of Fe−X bond covalency due to H-bonding with H_2O can be simulated by using point dipoles for the water molecules. For both the S^{2-} and the O^{2-} complexes the Fe−X bond covalency decreases significantly by 70% (i.e. the ligand coefficient decreases in the Fe^{III} 3d manifold from 81% to 69% in S^{2-} complex and from 73% to 57% in O^{2-} complex) of the decrease observed with H_2O molecules (Table 5). The rest of the decrease in the ligand coefficient appears to reflect the covalent charge transfer from the X^{2-} to the O−H σ^* orbitals of the H-bonded water molecules.[53] This indicates that the nature of the H-bonding interaction is mainly dipolar, in agreement with previous results, where the dipole stabilizes the charge on X^{2-} which reduces the covalency and weakens the Fe−X bond.[54] This is also evident from the increase of NPA charges on the X^{2-} ions on H-bonding (Table 5). These calculations also indicate that with both waters and point dipoles, the covalency is reduced in the π but not σ orbital (Table S2, Supporting Information). This reflects that the orientation of the dipoles toward the π donor orbitals of X, which stabilizes these π donor orbitals in energy and decreases their overlap with the Fe_{3d} orbitals, resulting in the observed reduction in Fe−X bond covalency.

D. Properties of a Hypothetical $Fe^{IV}-O$ Species. The electronic structure of an $Fe^{IV}-O$ complex with this ligand system, and the effects of H-bonding on it, have also been investigated using DFT calculations. The non-H-bonded complex is calculated to have an $S = 2$ ground state and a shorter (1.66 Å) and very covalent Fe−O bond relative to the Fe^{III} complex (93% vs 71% O_{2p} character, respectively). Compared to other non-heme $Fe^{IV}-O$ complexes, the Fe−O bond is longer (due to anionic amide donors) and the complex is high spin (due to the trigonal π donor ligand field). The $Fe^{IV}-O$ bond energy is about −187 kcal/mol, which is about 85 kcal/mol higher than the $Fe^{III}-O$ bond energy (−102 kcal/mol). Interestingly, the NPA charge on the oxo in $Fe^{IV}-O$ is almost neutral due to the increased covalency. High covalency leads to very weak H-bonding. The H-bonding energy of this complex is, in fact, less (calculated to be −1 kcal/mol in CH_2Cl_2 solvent) relative to an $Fe^{III}-O$ complex (−7 kcal/mol in CH_2Cl_2 solvent).[55] A bonding decomposition similar to Scheme 1 for the ferryl species shows that for $Fe^{IV}-O$, the H-bonding energy of one H_2O with the free O^{2-} (about −12 kcal/mol, Scheme S1, Supporting Information) is just enough to compensate for the loss of $Fe^{IV}-O$ bond energy (about 11 kcal/mol, as in Scheme S1) due to H-bonding and does not result in net stabilization.

Discussion

In this study XAS data and analysis have been used to evaluate results of DFT calculations on high-spin Fe^{III} oxo, sulfide, and hydroxo complexes of $[Fe^{III}H_3buea(X)]^{n-}$. The calculations are consistent with the XAS results and thus are used to evaluate Fe−X ($X = S^{2-}$, O^{2-}, and OH^-) bonding and the effects on H-bonding on Fe−S and Fe−O bonding.

The results show that although the Fe−S bond is more covalent (i.e. higher ligand character in the Fe_{3d} manifold) than the Fe−O bond, the Fe−O bond energy is much higher (−102 kcal/mol and −62 kcal/mol, respectively). From a simple MO description, the bond energy (BE) is given by $\alpha^2\Delta$, i.e. the covalency scaled by the energy of the ligand donor orbitals involved. Since oxo is more electronegative than sulfide, the O_{2p} orbitals are deeper in energy than the S_{3p} orbitals and thus though the total covalency of the oxo is lower it still has a larger covalent contribution to the bond energy. The strength of the Fe−O bond also has a significant contribution from the increased ionic nature of the Fe−O bond, which is facilitated by higher charge density on the oxo and shorter Fe−O bond length. This difference is estimated to be approximately 25 kcal/mol in the non-H-bonded complexes.[56]

Inclusion of H-bonds polarizes the Fe−X bonds and localizes charge density on X which weakens the Fe−X bond and results in lowering of the Fe−X bond energies, force constants, and covalencies. However, the overall H-bonding energy is favorable even with the weakened Fe−X bonds. Scheme 1 shows that this overall stabilization results from the compensation of the lowering the Fe−X bond energy by the large energy of H-bonding to the oxo/sulfido group. For both the oxo and sulfido

(49) The H-bonding energies are calculated from the dissociation energy of the $LFe^{III}-X$ complexes and the three water molecules (solvation corrected). The higher H-bonding energy for the $Fe^{III}-O$ complex is derived from shorter O···H distances and higher charge density on oxo relative to sulfido in the Fe−X complexes (Table 4).

(50) The thermal correction to enthalpy (including zero-point correction) was estimated for the Fe−O and the H-bonded Fe−O system to be +5 kcal/mol. The $T\Delta S$ contribution to the H-bonding (i.e. three water molecules to Fe−O) was estimated to be +31 kcal/mol at 300 K. Assuming that these values are comparable for the Fe−O and Fe−S systems, the ΔH for H-bonding is estimated (from the H-bonding ΔE's in Scheme 1) to be −19 kcal and −7 kcal and the ΔG is estimated to be +12 kcal/mol and +24 kcal/mol, respectively. These unfavorable ΔG's of H-bonding (due to the entropic term) indicate the preorganization role of the H_3buea chelate in lowering energy required for H-bonding.

(51) The H-bonding energies are calculated from the dissociation energy of the X^{2-} and the three water molecules having the same geometry as in the optimized $LFe^{III}-X + 3H_2O$ complex (solvent corrected).

(52) This is the interaction energy of a bare X^{2-} with three H_2O molecules having the same geometry as in the corresponding optimized H-bonded Fe^{III} complex calculated using the PCM method in CH_2Cl_2 solvent.

(53) Note that the covalent contribution in H-bonding is almost the same for both oxo and sulfido complexes. Although the sulfido has higher energy donor orbitals, it has lower S_{3p} character in those orbitals due to higher covalency of the Fe−S bond.

(54) Dey, A.; Okamura, T.-A.; Ueyama, N.; Hedman, B.; Hodgson, K. O.; Solomon, E. I. *J. Am. Chem. Soc.* **2005**, *127*, 12046−12053.

(55) Note that the H-bonding energy estimated here is for one H_2O molecule instead of the three H_2O in Table 5. The number of water molecules were reduced as the H-bonding between these H_2O molecules was complicating the geometry optimization of the H-bonded $Fe^{IV}-O$.

(56) Ionic interaction energy is estimated by treating the Fe, S, and O as point charges separated by their internuclear distances and the magnitude of the charges were derived from the NPA calculations.

complexes, the H-bond is mainly dipolar and selectively affects the Fe−X π bonds due to their favorable orientation with respect to the H-bonded dipoles. The Coulombic nature of the interaction leads to a stronger H-bond in the oxo complex due to its shorter O···HN H-bonding distance and high oxo charge, which in turn weakens the Fe−O bond more than the Fe−S bond upon H-bonding.

Terminal metal−oxo units are normally stabilized via multiple bonds between the metal ion and the oxo ligand. This type of bonding often produces low-spin complexes with relatively short M−O bonds. A recent proposal has suggested that in some cases H-bond(s) to the terminal oxo ligand could be used in stabilizing metal−oxo complexes.[18] The H-bonds would decrease the multiple bond character of the M−oxo unit, resulting in high-spin complexes with longer M−O bonds—properties such as those found in $[Fe^{III}H_3buea(O)]^{2-}$. These predictions are consistent with the results presented here. The properties of the $Fe^{III-}O$ bond, such as the reduced covalency and weakened Fe−O bond, are often associated with complex instability; however, in $[Fe^{III}H_3buea(O)]^{2-}$ they are offset by the overall stabilization gained via formation of the H-bonds.

The regulatory effects of H-bonds to terminal oxo ligands have been proposed to be important in metalloproteins. This proposal prompted us to examine the bonding in a related, but hypothetical, Fe^{IV-}oxo complex, containing $[H_3buea]^{3-}$ and one H-bonded H_2O molecule. The H-bonding energy in this $Fe^{IV}-O$ complex is significantly reduced (−1 kcal/mol) relative to the corresponding $Fe^{III}-O$ complex (−7 kcal/mol for 1 H_2O) due to strong covalency of the iron−oxo bond in the ferryl species, which reduces the charge on the oxo ligand.[57] This could be significant for Fe^{IV}═O intermediates in non-heme Fe enzymes. However, relatively little is known about these intermediates as only recently some low-spin models and a high-spin enzyme intermediate have been characterized.[58−61] However Fe^{IV}═O intermediates have been studied in heme systems. We calculate a similar weak H-bonding energy (∼ −0.7 kcal/mol) for an $Fe^{IV}-O$ porphyrin complex (with acetonitrile as the axial ligand) for both the S = 2 state (for direct comparison with the non-heme system) and S = 1 state (experimental ground state). This indicates that the very covalent $Fe^{IV}-O$ bond in both heme and non-heme ligand environments allows for only weak H-bonding. However, using resonance Raman spectroscopy at different pH's, effects of H-bonding by a protonated histidine residue have been observed.[62] With a charged imidazole, the calculated H-bonding energy of the heme $Fe^{IV}-O$ species increased to −6.2 kcal/mol. For a non-heme $Fe^{IV}-O$ group this is calculated to be −10.1 kcal/mol.[63] This suggests that for a significant H-bonding interaction with an Fe^{IV}═O species (heme or non-heme) the donor should be protonated.

Table 6. Calculated H-bonding Energies for Ferryl Complexes

	Fe–O (Å)	q_{Fe}[a]	q_O[a]	H-bonding energy[b]
$Fe^{III}-O$ (L)[c]	1.74	2.44	−0.01	
$Fe^{III}-O$ (L) + H_2O	1.76	2.50	−0.17	−7.3
$Fe^{IV}-O$ (L)				
S = 2	1.66	1.86	0.10	
$Fe^{IV}-O$ (L) + H_2O				
S = 2	1.67	1.88	0.02	−1.4
$Fe^{IV}-O$ (L) + ImH^+				
S = 2	1.68			−10.1
$PFe^{IV}-O(CH_3CN)$[d]				
S = 1	1.63	0.96	0.22	
S = 2	1.64	1.96	0.21	
$PFe^{IV}-O(CH_3CN)$ + H_2O				
S = 1	1.64	0.99	0.18	−1.4
S = 2	1.64	2.00	0.09	−0.7
$PFe^{IV}-O(CH_3CN)$ + ImH^+				
S = 2	1.65			−6.2

[a] NPA charges. [b] Values in kcal/mol computed using a PCM model. [c] L stands for the modified H_3buea ligand where the H-bonding arms are truncated. [d] P stands for an unsubstituted porphirinato ligand.

In summary, the $Fe^{III}-O$ bond is stronger than that of an $Fe^{III}-S$ bond due to the ionic contribution that also leads to the stronger H-bonding interaction of the $Fe^{III}-O$ species. Upon oxidation, the $Fe^{IV}-O$ is highly covalent which reduces the charge on the oxo ligand and decreases its ability to H-bond.

Acknowledgment. This research was supported by NIH Grants GM 0446304 (E.I.S.), RR-01209 (K.O.H.), and GM50781 (A.S.B.). SSRL is supported by the Department of Energy, Office of Basic Energy Sciences. The SSRL Structural Molecular Biology Program is supported by the National Institutes of Health, National Center for Research Resources, Biomedical Technology Program, and by the Department of Energy, Office of Biological and Environmental Research. R.K.H. thanks Dr. Serena DeBeer George and Mr. Patrick Hillyard for their assistance in measuring the Fe K-edge XAS data.

Supporting Information Available: Fits to the Fe K-edge XAS data, coordinates of all optimized geometries, π and σ deconvolution of the covalencies, and bonding scheme for $Fe^{IV}-O$ are available free of charge from http://pubs.acs.org.

JA061618X

(57) Separate DFT optimizations done with one H_2O molecule.
(58) Klinker, E. J.; Kaizer, J.; Brennessel, W. W.; Woodrum, N. L.; Cramer, C. J.; Que, L. J. *Angew. Chem., Int. Ed.* **2005**, *44*, 3690−3694.
(59) Rohde, J.-U.; In, J. H.; Lim, M. H.; Brennessel, W. W.; Bukowski, M. R.; Stubna, A.; Münck, E.; Nam, W.; Que, L., Jr. *Science* **2003**, *299*, 1037−1039.
(60) Price, J. C.; Barr, E. W.; Tirupati, B.; Bollinger, J. M., Jr.; Krebs, C. *Biochemistry* **2003**, *42*, 7497−7508.
(61) Riggs-Gelasco, P. J.; Price, J. C.; Guyer, R. B.; Brehm, J. H.; Barr, E. W.; Bollinger, J. M., Jr.; Krebs, C. *J. Am. Chem. Soc.* **2004**, *126*, 8108−8109.
(62) Mukai, M.; Nagano, S.;Tanaka, M.; Ishimori, K.; Morishima, I.; Ogura, T.; Watanabe, Y.; Kitagawa, T. *J. Am. Chem. Soc.* **1997**, *119*, 1758−1766.
(63) Note that the H-bonding energy with a positively charged imidazole ring and a negatively charged $Fe^{IV}-O$ unit may be overestimated by additional Coulombic interaction.